The International Journal of Advanced Manufacturing Technology
https://doi.org/10.1007/s00170-024-14412-y

ORIGINAL ARTICLE

Optimization of multi-axis laser shock peening process for nickel alloy components based on workpiece curvature and equipment dynamic performance

Ri Pan[1] · Yun Xing[1] · Rui Wang[1] · Jinwei Fan[1] · Dongju Chen[1] · Kun Sun[1] · Peng Gao[1]

Received: 26 April 2024 / Accepted: 5 September 2024

Abstract
Nickel alloys are widely used in aerospace and defense industries due to their excellent high-temperature characteristics. In order to increase fatigue resistance and oxidation corrosion resistance, aerospace curved surface parts always need to be strengthened using laser shock peening technology on five-axis machines. However, it is easy to generate dense laser spots in certain regions during the process, which might lead to an uneven distribution of residual stress on surfaces of the component. To address this issue, the study investigates the problem of excessive spot overlap rate at large curvature positions caused by a mismatch between the surface curvature of curved components and the dynamic performance of equipment, then proposes an optimization algorithm for motion control based on linear interpolation principles. By analyzing the relationship between the feed rate of the program segment and the actual feed rate, the speed of each axis of the machine tool is confirmed and adjusted, and the control flow of the optimization algorithm is established. The feasibility of the algorithm is preliminarily verified by comparing the changing trend of feed rate before and after optimization through simulation. In actual laser shock peening experiments on nickel alloy spherical shell elements, the laser spot distribution on the surface of the component is uniform, and the relative error range between the actual overlap ratio and the theoretical value can be controlled within 5%, demonstrating the correctness of the optimization algorithm. This study can significantly improve the surface machining quality of curved components and have practical applications.

Keywords Nickel alloy · Laser shock peening · Five-axis linkage · Motion control optimization

1 Introduction

In the field of aerospace and defense, nickel-based superalloys are widely used in the manufacture of turbine blades, combustion chambers, and other key hot-end components of aeroengines at operational temperatures higher than 550 ℃. This is due to their good corrosion resistance, high strength at high temperatures, excellent creep fatigue resistance, and long fatigue life [1–4]. At present, with the continuous improvement of performance requirements for aero-engines, it is necessary to improve the high-temperature mechanical properties of materials used to manufacture aero-engines, especially high-temperature oxidation resistance, corrosion resistance, and fatigue resistance. Therefore, it is essential to carry out an efficient and stable surface hardening treatment for nickel alloy components.

Traditional methods of surface strengthening of metallic materials mainly include surface mechanical strengthening, surface heat treatment strengthening, chemical heat treatment strengthening, surface laser cladding treatment, and surface electron beam treatment [5]. However, these methods are energy-intensive and complex. Laser shock peening (LSP) method is a surface modification technology. In this method, metallic materials are irradiated by high-power lasers to produce high-temperature and high-pressure plasma, which impact the surface of material to change its surface properties through mechanical effects [6]. And then the fatigue [7, 8] and corrosion resistance [9, 10] of the materials can be improved. It has the advantages of high processing efficiency, a clean working environment, and precise control of process parameters [11]. As a novel

✉ Peng Gao
gaopeng_bjut@126.com

[1] Beijing Key Laboratory of Advanced Manufacturing Technology, Beijing University of Technology, Beijing, China

Published online: 19 September 2024

surface-strengthening technology, applications of laser shock peening in the industrial field have been reported [12–16], and at the same time, research in the academic community has also been conducted [17–20]. All of these factors have promoted the wide application of laser shock peening technology in the machining of curved surface components of aeroengines.

Nowadays, laser shock peening is mainly completed using machine tools. Note that the key components of aeroengines are generally complex curved surfaces, which result in ordinary three-axis machine tools not meeting the laser shock peening processing requirements of aero-engine components. With the increasing progress and popularity of equipment, laser shock peening technology based on five-axis machine tools has been proposed and applied. Five-axis machine tools can better adapt to the processing of complex surfaces, expanding the scope of application of laser shock peening. For example, it has been investigated as one of the important methods for surface peening of nickel alloys [21–23].

In the actual use of machine tools for strengthening processing, to ensure good strengthening effect, it is necessary to keep the actual feed rate constant under ideal processing conditions. This requirement can be met by setting the feed rate to a fixed value in the program segment of the ordinary three-axis machining system. The common solution is to optimize the algorithm of the processing system and dynamically adjust the feed rate in the actual processing process to avoid the change of spot overlap rate. Sang et al. [24] presented an improved feed rate scheduling method by calculating the geometric error between the real tool path and the ideal tool path and building the constrained feed rate profile. Sun et al. [25] proposed a toolpath smoothing algorithm to eliminate feed rate fluctuation within the feed rate planning units. Tang et al. [26] developed a novel master-based feed rate scheduling (MBFS) approach with real-time and drive constraints to generate smooth trajectories along five-axis linear toolpaths.

However, for the five-axis machining system, to position the laser on workpieces more accurately, two rotary axes are introduced to provide additional degrees of freedom. When the five-axis machining system is applied to perform laser shock peening on workpieces with complex surface profiles, the rotation angle of two rotary axes is supposed to change in real time according to the curvature of the machining trajectory to maintain a stable overlapping ratio and ensure the laser is perpendicular to the surface consistently. This means the feed rate is not allowed to be constant. In other words, optimizing the feed rate based on the curvature of the machining trajectory during laser shock peening processing is necessary [27]. Unlike the traditional three-axis machines, for five-axis machines, two rotary axes are expected to rotate with a larger angle than usual when reaching an area with large curvature during the single interpolation process. Unfortunately, when the feed rate remains constant, the rotation angles of rotary axes cannot be adjusted timely, which results in the target point of the laser shock not being able to move from the previous position to the next specified position in time. This situation occurs in dense spots on the surface generating thermal deformation and residual stress, which seriously affects the actual machining quality and productivity.

To solve this problem, this paper researches the five-axis linkage surface machining process for laser shock processing of nickel alloy. Through the understanding of the principle of laser shock processing and combining the five-axis linkage and linear interpolation principle, the relationship between the program segment feed rate and the actual feed rate was analyzed. The relevant algorithm to combine the feed rate with the actual motion position is designed. Ensure the laser shock processing effect by rationally changing the feed rate. This research can effectively solve the dense spot situation of curved components and improve the surface processing quality of components. The study advances the research of motion control technology of multi-axis laser processing equipment and provides a technical basis for improving the multi-axis processing effect of laser processing of complex feature parts.

2 Study on motion control optimization of laser shock process for nickel alloy curved components

2.1 Problem statement

On the surface strengthening treatment of metal workpieces in the aviation engine, the following study takes nickel-based high-temperature alloys as the object of research and laser shock peening as the processing technology. Problems in laser shock peening of nickel alloy workpieces on multi-axis laser processing equipment are mainly investigated.

2.1.1 Laser shock peening principle for curved components

The principle diagram of laser shock peening of a nickel alloy spherical shell part is shown in Fig. 1(a). According to the path planning for the hemispherical shell, multiple machining points with the same spacing are obtained. In the direction of the normal vector of the machining points, the pulsed laser of the multi-axis precision machining equipment emits a laser beam through the lens to the workpiece machining points. The laser beam irradiates the surface of the workpiece to form a spot with a certain diameter.

In the laser impact strengthening process mentioned above, different process parameters will affect the

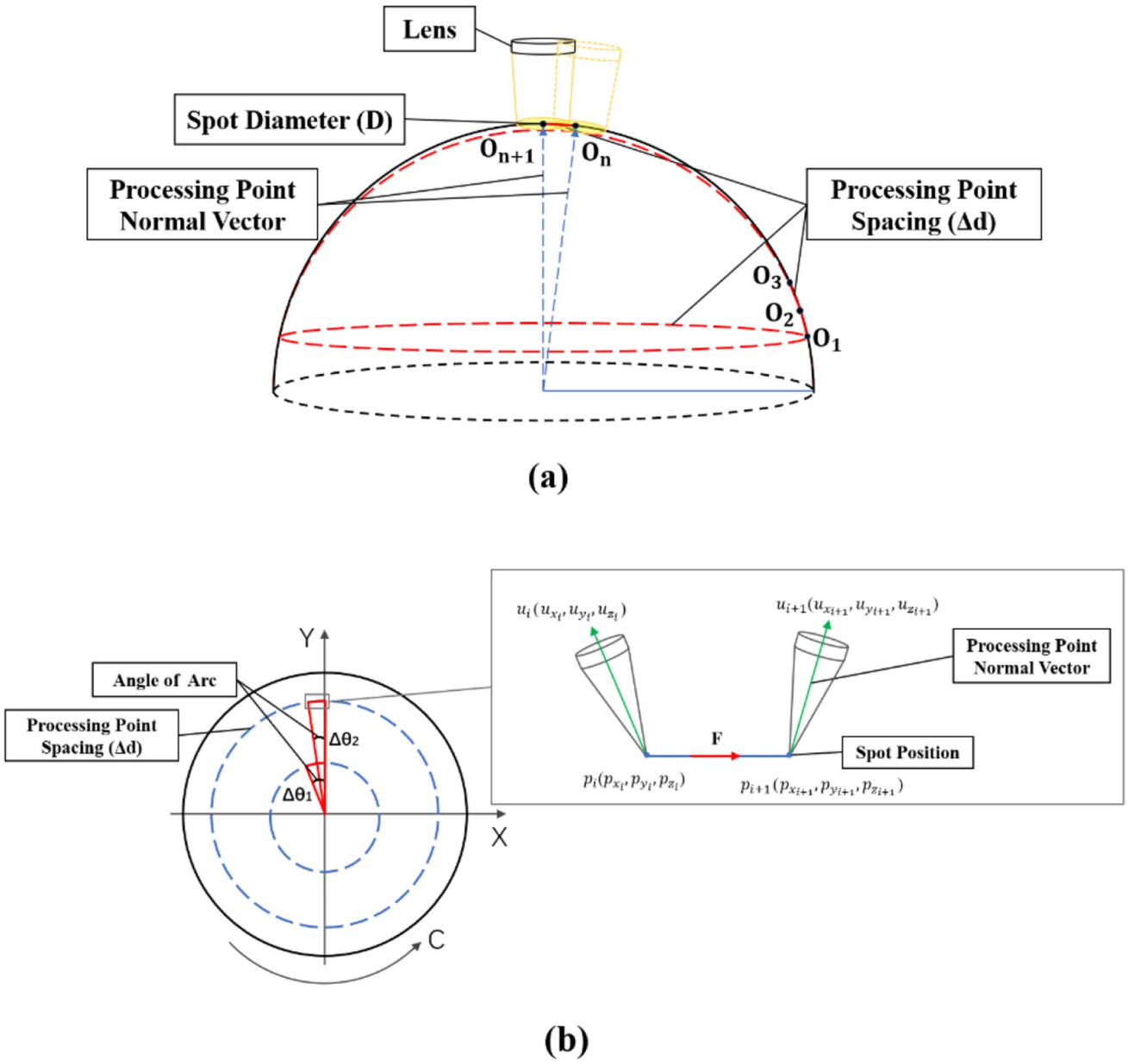

Fig. 1 Schematic diagram of laser shock peening of nickel alloy

strengthening effect, among which the spot overlap ratio is an important parameter affecting the surface strengthening effect. Suitable and uniform spot overlap ratios can increase the residual compressive stress in the surface layer of the material and result in a more uniform distribution of residual stresses on the surface of the material.

The spot overlap ratio (η) is defined as the ratio of the overlap distance between two adjacent spots on the centerline (L_0) and the spot diameter (D), as shown in Fig. 2. The value will be used as an input parameter for the laser-intensified processing path generation algorithm, affecting the spacing between the processing points. Thus, it has an impact on the stress field distribution in the laser shock region [28], which ultimately directly affects the effect of laser shock peening.

During the machining process, the spot overlap ratio and spot diameter are used as input parameters to directly affect the spacing between neighboring machining points (Δd) in the machining path, which are related as:

$$\Delta d = D \times (1 - \eta) \tag{1}$$

When generating machining points on the sphere, it is theoretically necessary to ensure that the machining points

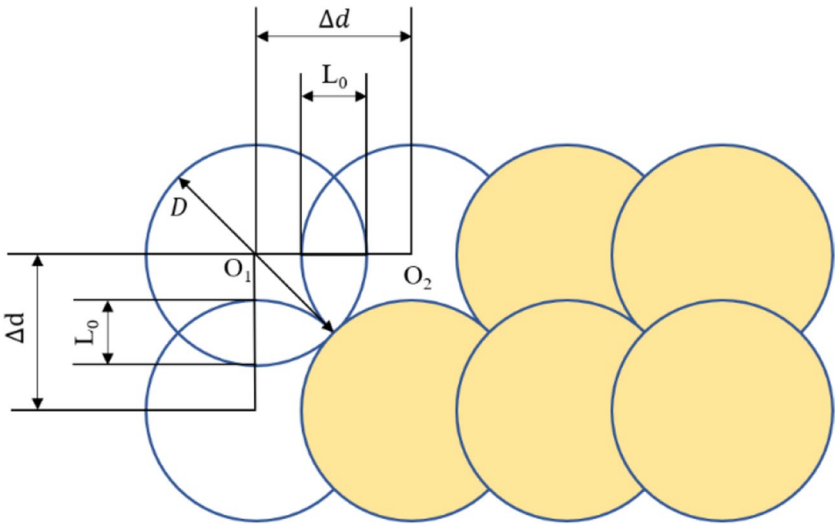

Fig. 2 Spot overlap ratio

are equally spaced along the circumference and the busbar. Therefore, the sphere is stratified along the direction of the busbar according to the equal processing point spacing generated by the calculation of (1), which leads to the points O_1, O_2……O_{n+1} in Fig. 1(a). After layering, the individual circumference continues to be divided by equal machining point spacing (Fig. 1(a) red dotted line) and finally generates all the processing points of the sphere.

2.1.2 Motion control analysis of laser shock peening of curved components

Typically, surface enhancement machining is done with uniform feeds. However, maintaining a constant feed rate on a five-axis machine can lead to the problem of dense spotting at some locations of the curved component, which affects the machining results. The laser shock peening process uses constant frequency processing. In order to ensure the laser overlap ratio, the ideal processing situation should be that the laser corresponds to one pulse of light for each moving path of the motion platform with a point spacing of Δd size. Based on the correspondence, the moving speed (F) of the laser outlet is the displacement generated per unit time:

$$\begin{aligned} F &= \Delta d/T \\ &= D \times (1-\eta) \times f \end{aligned} \tag{2}$$

The feed rate obtained by the calculation of (2) describes the ideal moving speed of the spot relative to the surface of the workpiece in the workpiece coordinate system. However, during the actual machining of the nickel alloy spherical shell parts, the machining path of the spherical shell is processed layer by layer according to different radius circumferences. The radius of the circumferential path decreases and the curvature increases in the part near the top of the spherical shell. According to the definition of curvature of curve in (3), it can be seen that the amount of angular variation ($\Delta\theta$) between neighboring machining points increases when the curvature (k) increases due to the constant machining point spacing (Δd).

$$k = \left|\frac{\Delta\theta}{\Delta d}\right| \tag{3}$$

where k is the mean curvature of the curve, Δd is the arc length of the curve, and $\Delta\theta$ is the tangent angle of the arc.

As shown in Fig. 1(b), it is the top-view schematic of hemispherical shell machining, where the red dotted lines represent the circumferential machining paths at different radii. As the circumferential radius decreases, there is the amount of angular change $\Delta\theta_1 > \Delta\theta_2$ per unit step.

The motion of the B-C rotary table five-axis linkage laser machining platform used in this paper is analyzed as shown in Fig. 3. By establishing the machine kinematic chain, the positive kinematic solution equation can be obtained when the laser platform processing to a certain processing point in the path [29]:

$$\begin{bmatrix} u_x \\ u_y \\ u_z \\ 0 \end{bmatrix} = \begin{bmatrix} -sin(\theta_B)cos(\theta_C) \\ sin(\theta_B)sin(\theta_C) \\ cos(\theta_B) \\ 0 \end{bmatrix} \tag{4}$$

where θ_B is the rotation angle of the B rotation axis, and θ_C is the rotation angle of the C rotation axis. The $u(u_x, u_y, u_z)$ is the laser vector in the workpiece coordinate system.

The processing point laser vector is the unit normal vector to the surface of the spherical shell, so its value is a partial derivative of the spherical equation:

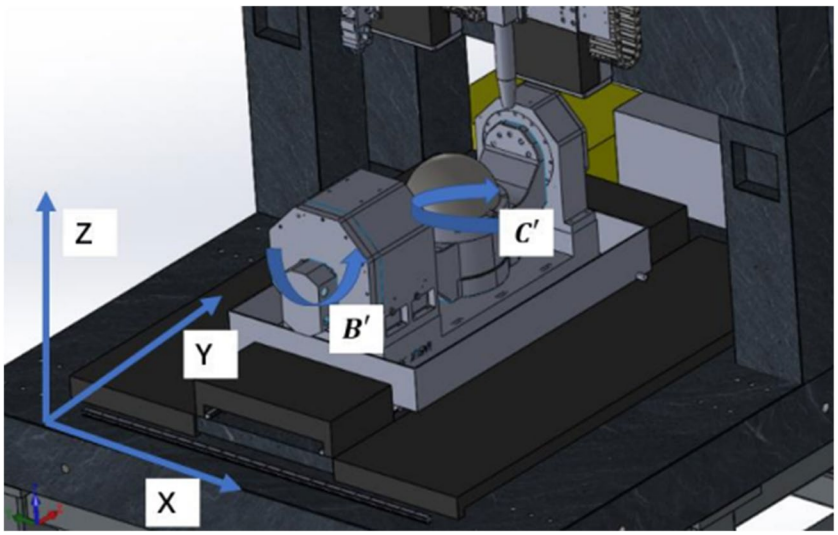

Fig. 3 Structure of five-axis laser processing platform

$$\begin{cases} u_x = \frac{2p_x}{u_x^2+u_y^2+u_z^2} \\ u_y = \frac{2p_y}{u_x^2+u_y^2+u_z^2} \\ u_z = \frac{2p_z}{u_x^2+u_y^2+u_z^2} \end{cases} \tag{5}$$

where, p_x, p_y, p_z, are the coordinate values under the workpiece coordinate system of the machining point.

Combined with (4) and (5) gives the relationship between the rotation angle of the rotary axis C and the position of the machining point:

$$\tan\theta_C = -\frac{p_y}{p_x} \tag{6}$$

where the value of $\frac{p_y}{p_x}$ can be considered as the slope of the line between the point to be machined and the center of the circle in the forward top view of the Z-axis of the spherical shell. As the amount of angular change between adjacent processing points increases, the amount of change in $\frac{p_y}{p_x}$ also increases. This causes the theoretical instantaneous rotation angle of the C-axis ($\Delta\theta_c$) to increase. The required instantaneous speed of the C-axis will exceed the machine setting when the value of $\Delta\theta_c$ is too large.

Figure 4 shows the machining effect of setting the constant feed rate of the program segment. When the radius of the circumference being machined decreases, the C-axis partial speed cannot meet the instantaneous corner demand, and thus the specified attitude cannot be reached within one interpolation cycle. This resulted in the dense spotting and excessive overlap ratios near the top of the spherical shell shown in the portion. This situation is likely to lead to uneven distribution of residual stresses on the surface, affecting the overall machining quality of the component.

Fig. 4 Actual effect of machining at a constant feed rate

Therefore, this paper focuses on how to design relevant algorithms to combine the feed rate with the actual motion position in the five-axis linkage machining process, and reasonably control the size of the feed rate to ensure the effect of laser shock peening.

2.2 Motion control optimization for laser shock peening of curved components

2.2.1 Process of motion control optimization algorithm

According to the above analysis, in order to solve the problem of dense spot caused by curved components and feed rate, a five-axis linkage motion control optimization algorithm was designed to calculate the feed rate of different positions of the laser processing equipment in practical work. Figure 5 shows the flow chart of the motion control strategy.

The main idea of the motion control optimization algorithm is specifically divided into the following steps:

Step 1. According to the planning of hemispherical shell machining path to get the machining point position information $(p_x, p_y, p_z, u_x, u_y, u_z)$. And solve to get the coordinates of the machining point under five-axis linkage (X, Y, Z, B, C).

Step 2. Calculate the actual synthesized displacement (ΔL), the distance between two adjacent path points (Δd), and the ideal constant feed rate (F_0) in linear interpolation.

Step 3. Calculate the actual five-axis linkage feed rate according to the above results. And calculate partial speed $(F_X, F_Y, F_Z, F_B, F_C)$ of each axis according to the principle of linear interpolation.

Step 4. The speed check is carried out to compare the sub-speed of each axis of the machine tool with the limit speed of the machine tool. Correcting the feed rate through the correction formula when the partial speed of an axis of motion exceeds the permissible range of the machine.

Step 5. Determine whether it is the last processing point. If so, end the algorithm, otherwise go to step two.

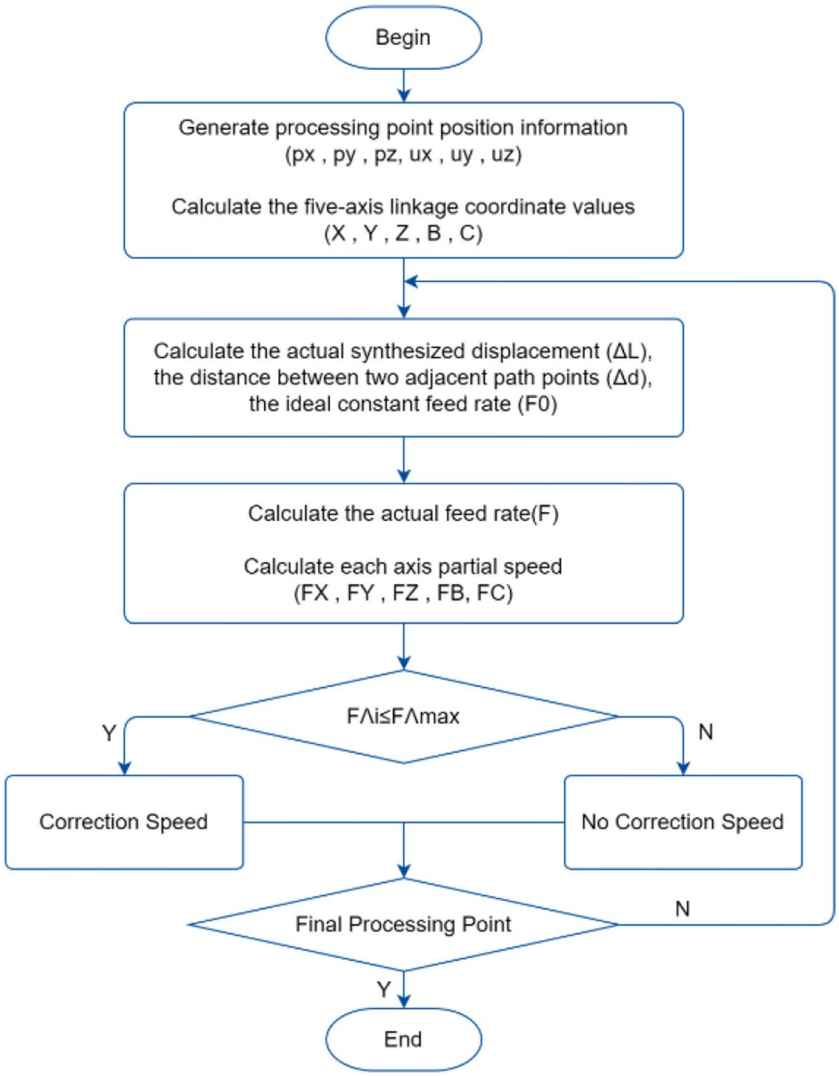

Fig. 5 Flow chart of the five-axis motion control strategy

2.2.2 Calculation and correction of feed rate

For the above algorithmic process, in five-axis linkage machining, the trajectory of the machining points on the machined surface is discretized into numerous tiny straight-line segments. The trajectory direction and coordinates are controlled using G01 linear interpolation of the CNC.

Assuming that the laser position information of two adjacent machining points in five-axis machining are $(p_{x_1}, p_{y_1}, p_{z_1}, u_{x_1}, u_{y_1}, u_{z_1})$ and $(p_{x_{i+1}}, p_{y_{i+1}}, p_{z_{i+1}}, u_{x_{i+1}}, u_{y_{i+1}}, u_{z_{1i+}})$ shown in Fig. 1(b). The coordinate values of the machine tool in the corresponding CNC program are respectively $(X_i, Y_i, Z_i, B_i, C_i)$ and $X_{i+1}, Y_{i+1}, Z_{i+1}, B_{i+1}, C_{i+1}$, and the actual displacements of each translational and rotary axis of the machine tool is $(\Delta X, \Delta Y, \Delta Z, \Delta B, \Delta C)$. According to the principle of linear interpolation, the synthetic displacement of the laser linear interpolation program segment between the line segments is:

$$\Delta L = \sqrt{(\Delta X)^2 + (\Delta Y)^2 + (\Delta Z)^2 + (K_b \Delta B)^2 + (K_c \Delta C)^2} \tag{7}$$

where K_b is the adjustment factor for converting the rotation angle of the B-axis to displacement length. K_c is the adjustment factor for converting the rotation angle of the C-axis to displacement length.

The distance between two adjacent machining path points on the machining path in the workpiece coordinate system is:

$$\begin{aligned} \Delta d &= \sqrt{(\Delta p_x)^2 + (\Delta p_y)^2 + (\Delta p_z)^2} \\ &= \sqrt{(p_{x_{i+1}} - p_{x_i})^2 + (p_{y_{i+1}} - p_{y_i})^2 + (p_{z_{i+1}} - p_{z_i})^2} \end{aligned} \tag{8}$$

Let the ideal constant feed rate (F_0) of the laser spot be calculated from (2) based on the actual spot parameter requirements. The value of the program segment feed rate F instruction (F_s) represents the displacement generated per unit time. Combined with (7) and (8), the program segment feed rate (F_s) has the following relationship to the actual feed rate (F_0):

$$\begin{aligned} F_s &= \frac{\Delta L}{\Delta d} F_0 \\ &= \frac{\sqrt{(\Delta X)^2 + (\Delta Y)^2 + (\Delta Z)^2 + (K_b \Delta B)^2 + (K_c \Delta C)^2}}{\sqrt{(\Delta p_x)^2 + (\Delta p_y)^2 + (\Delta p_z)^2}} F_0 \end{aligned} \tag{9}$$

According to the principle of linear interpolation, the commanded value of feed rate (F_s) is the synthesized speed of the partial speed of the motion of each axis of the machine, and the interpolation period of each axis is equal:

$$\frac{|\Delta X|}{F_X} = \frac{|\Delta Y|}{F_Y} = \frac{|\Delta Z|}{F_Z} = \frac{|\Delta B|}{F_B} = \frac{|\Delta C|}{F_C} = \frac{\Delta L}{F_s} = T \tag{10}$$

$$\begin{cases} F_X = \frac{|\Delta X|}{\Delta L} F_s \\ F_Y = \frac{|\Delta Y|}{\Delta L} F_s \\ F_Z = \frac{|\Delta Z|}{\Delta L} F_s \\ F_B = \frac{|\Delta B|}{\Delta L} F_s \\ F_C = \frac{|\Delta C|}{\Delta L} F_s \end{cases} \tag{11}$$

where F_X (mm/min), F_Y (mm/min), F_Z (mm/min), F_B ((°)/min), and F_C ((°)/min) are the component speeds of the laser processing equipment in each axis of motion.

Due to the limitations of the dynamic performance of the equipment, there are limits to the maximum speed and acceleration of the axes of the actual laser processing equipment. If the speed of an axis exceeds its servo capacity range after the program speed decomposition, it will cause an axis of the machine to fall out of step and not be able to reach the specified position, thus creating a large machining error. Therefore, the five-axis linkage process needs to be based on the machine's limit speed index of the machine tool axis of the sub-speed of the verification and correction to ensure that the feed rate in the axes of motion of the sub-speed can not exceed the maximum speed, that is:

$$F_{\wedge i} \le F_{\wedge \max} (\wedge = X, Y, Z, B, C) \tag{12}$$

where $F_{\wedge i}$ is the partial velocity of a particular axis of motion. $F_{\wedge \max}$ is the maximum velocity of a particular axis of motion.

When the partial speed of each axis of motion exceeds the allowable range of the machine tool, it is necessary to correct the feed rate. At this time, the maximum speed of the machine tool motion axis is taken to obtain the new feed rate of the axis. The actual speeds of the remaining axes are based on the time of motion of the limiting axes. The correction formula for the feed rate is:

$$F = \min \left\{ F_{\wedge \max} \frac{\Delta L}{|\Delta \wedge|} \right\} (\wedge = X, Y, Z, B, C) \tag{13}$$

This completes the correction of the feed rate of the program segment and the whole process of the motion control optimization algorithm. According to the above process and calculation results, the corresponding surface path processing code is generated.

3 Simulation analysis and experimental verification

3.1 Simulation analysis

To verify the effectiveness of the motion control optimization algorithm proposed in this paper, simulation, and comparison experiments are carried out.

According to the above five-axis linkage motion control algorithm, the ideal constant feed rate of the R50 hemispherical shell is set. The relevant program is formed to obtain the feed rate corresponding to each program segment of laser shock peening. The simulation results are shown in Fig. 6. Comparing the feed rate analysis before and after optimization in the figure. It can be seen that when the impact strengthens to the top of the spherical shell, the feed rate of the corresponding program segment is significantly improved compared to the constant feed rate.

Then, the speed changes of the laser processing platform before and after the optimization of the sub-velocity of each axis are analyzed, as shown in Fig. 7. The blue line in the figure is the partial speed of each axis under the ideal constant feed rate before optimization, and the red line is the partial speed of each axis after adopting the motion control optimization algorithm. Some of the red lines are covered by the blue lines. From the figure, it can be seen that the trend of partial speed before and after optimization of the X, Y, Z, and B axes is unchanged, and the partial speed after optimization is slightly higher than that before optimization. The C-axis partial speed changes greatly before and after optimization. The C-axis partial speed remains almost constant at a constant feed rate. The partial speed after the optimization algorithm increases as the radius of the circle

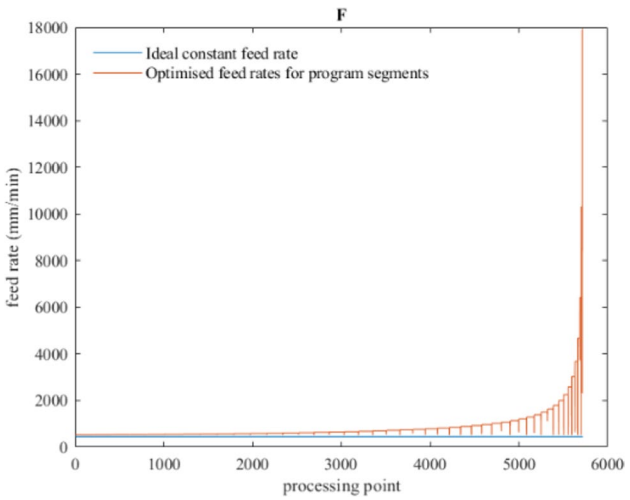

Fig. 6 Distribution of feed rate in the machining program segment

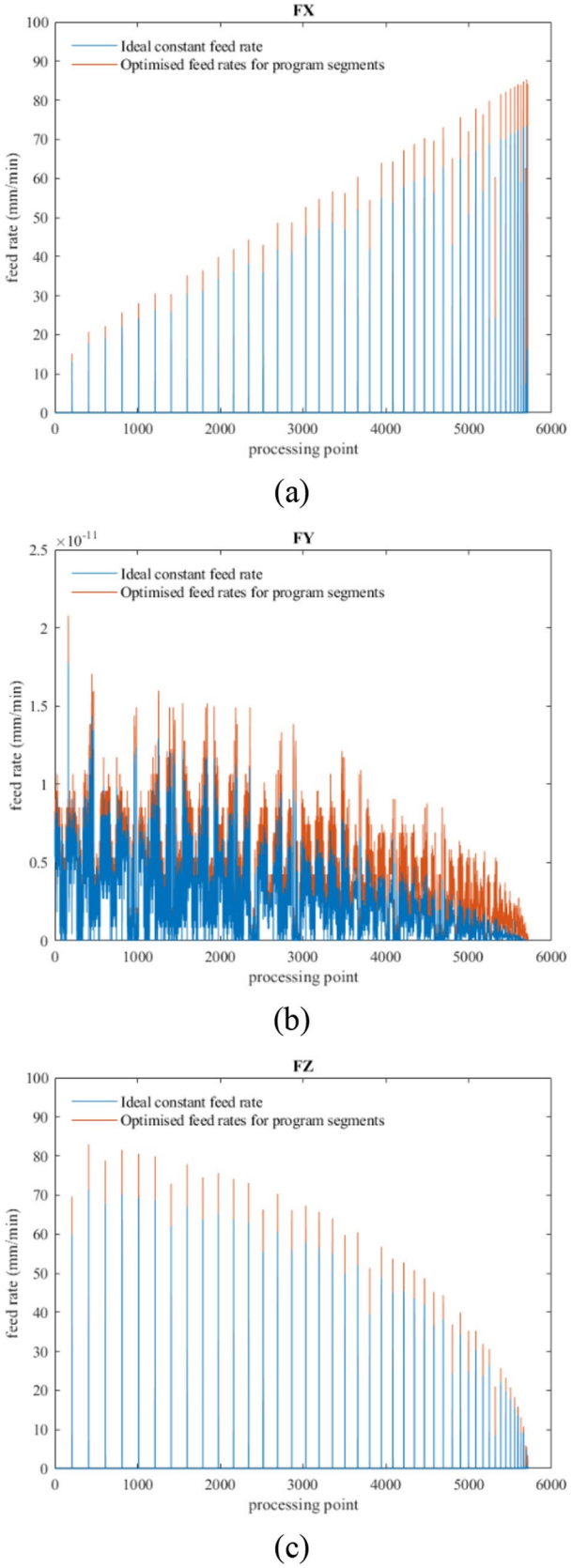

Fig. 7 Partial speed of each axis before and after optimization

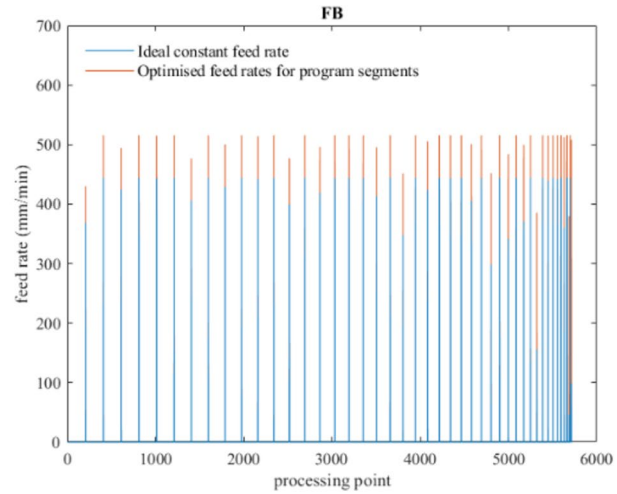

(d)

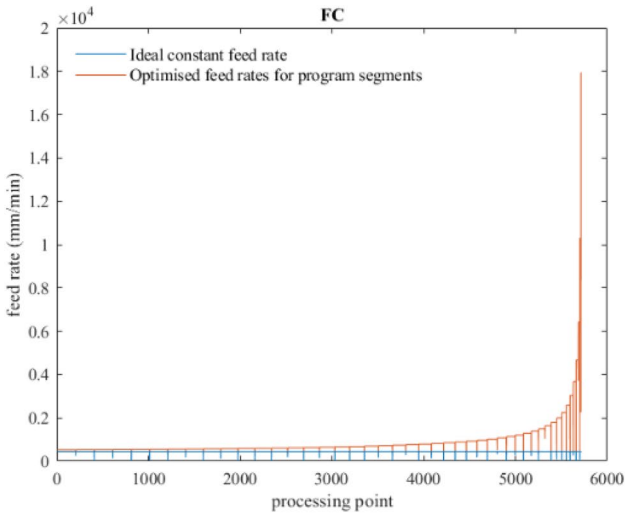

(e)

Fig. 7 (continued)

on the path decreases, which better meets the demand when the instantaneous angle increases.

The simulation results preliminarily verify the feasibility of the five-axis linkage motion control optimization algorithm.

3.2 Experiments design

3.2.1 Experimental conditions

Figure 8(a) shows the precision laser shock peening experimental site. The precision laser processing equipment used in the experimental site is a combination of laser shock peening technology, numerical control technology, and precision

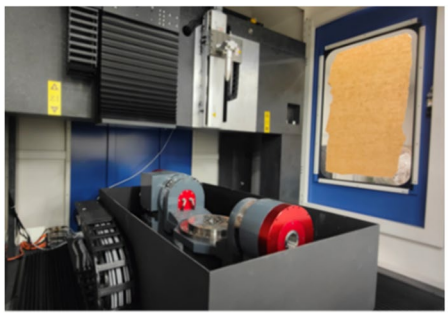

(a)

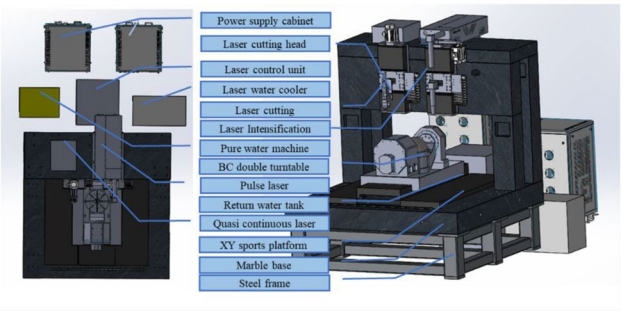

(b)

Fig. 8 Multi-axis precision laser shock peening equipment

monitoring and testing technology of high-end processing equipment.

The equipment has four linear axes and two rotary feed axes for motion control, as shown in Fig. 8(b). The X-axis and Y-axis realize the horizontal translation movement of the workpiece, and the B-axis and C-axis provide the spatial position rotation of the tooling, fixtures, and parts. The Z1-axis and Z2-axis provide translational motion in the vertical direction for the laser microfabrication system and the laser shock peening system, respectively.

This experiment only involves the movement of the Z2 axis in the vertical direction, so the equipment is actually a "six-axis five linkage" motion system, which belongs to the B-C rotary table type five-axis linkage machine tool.

Figure 9 illustrates the preparation prior to laser shock peening. The deionized water machine is controlled by a PLC as in Fig. 9(a). The deionized water forms an absorbing layer on the surface of the target and is used to confine the shock wave generated by the plasma explosion. The surface of the spherical shell made of nickel alloy material clamped on the fixture is uniformly covered by black aluminum foil tape, as shown in Fig. 9(b). The black aluminum foil tape absorbs the plasma generated by the laser energy to protect the target. It also helps to show the surface paths of the target after impact intensification and facilitates observation and measurement of the experimental results.

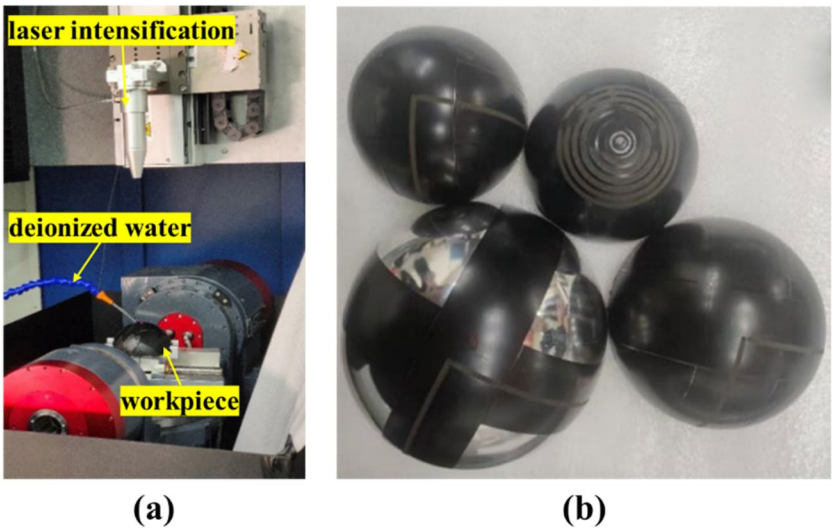

Fig. 9 Preparation for laser shock peening experiments

Table 1 Constant feed rate machining parameter table

Radius of spherical shell (mm)	Spot diameter (mm)	Spot overlap ratio	Edge reservation (mm)	Processing path	Pulse frequency (Hz)	Pulse energy density (J)
50	3	25%	20	Isotropic grating	5	800

3.2.2 Experimental procedure

This experiment requires setting parameters such as spot size, spherical shell radius, overlap rate, and edge reservation in the program before the experiment to generate the machining path and motion axis coordinates. Then set the laser pulse frequency during machining, and calculate the ideal feed rate according to (2). And set the feed rate before and after optimization respectively in the NC program. The NC program is imported from the host computer software into the control system for laser shock peening during the experiment.

After the experiment, the results of the machining of the parts need to be measured, calculated, and analyzed. Due to the large number of light spots in the machining path, the experiment uses vernier calipers to randomly measure the spot size at any machining point in the machining path. The expectation and variance are obtained to measure whether the actual spot size meets the machining expectation. Similarly, the overlap length of the two spots along the circumferential direction is measured randomly at any processing point in the path, and the actual overlap ratio at the processing point is calculated by the lap ratio formula.

Based on the above experimental steps, experiments were designed to compare the machining effects of uniform and optimized feed rates respectively.

Fig. 10 Effect of constant feed rate machining of nickel alloy spherical shells

(1) Constant feed rate experiment

The parameters of laser impact intensified machining of the spherical shell were set before the experiment, and the values of each parameter are shown in Table 1.

The ideal feed rate was calculated as 675 mm/min according to (2) and was set as a constant feed rate in the NC program. The surface machining effect of the spherical shell after laser shock peening is shown in Fig. 10.

Table 2 Measurement results of machining at a constant feed rate

Mean actual spot diameter (mm)	Sample variance of spot diameter	Sample variance of spot overlap ratio	Actual edge reservation (mm)
3.00	0.0196	0.0350	20

Twenty random samples were selected for the surface measurements of the machined spherical shells in Fig. 10, and the results are shown in Table 2.

The experimental results show that the actual spot size remains uniform along the overall machining path direction, and there is no obvious deviation from the set value. The measured actual edge reservation length is also consistent with the set value in the path planning.

However, the actual spot overlap ratio has a large deviation from the ideal value. From the bottom to the top of the spherical shell along the direction of the busbar, the actual spot overlap ratio is getting larger and larger. At the same time, at the top of the spherical shell, due to the mismatched slower feed rate, there is a situation where the laser impact breaks the tape.

The constant feed rate processing experiment shows that if a constant feed rate is used for laser shock peening, the actual laser overlap ratio will not meet the ideal processing requirements.

(1) Experiment for optimized motion control

The five-axis linkage motion control optimization algorithm based on laser shock peening designed in this paper was used for the experiments. Three groups of motion control optimization experiments under different condition parameters and one group of constant speed control experiments were done. The relevant settings of processing parameters in the four groups of experiments are shown in Table 3.

Figure 11 shows four groups of spherical shell laser shock peening effect, respectively, along the direction of the spherical shell processing path randomly selected processing points. Set the processing point sample capacity of 20, and measure the actual spot size and spot overlap ratio at the processing point (Appendix). The spot diameter and spot overlap ratio measurements are shown in the form of line graphs in Fig. 12 and Fig. 13, where the blue line is the result of the four groups of experiments and the orange line is the theoretical parameter value.

According to the analysis of the actual spot diameter data in Fig. 12, the relative error between the actual spot diameter of the experiments and the theoretical setting value is small. So either using an optimized feed rate or a constant feed rate, the actual spot size can be processed with less error from the theoretical value.

The actual spot overlap ratio data is shown in Fig. 13. It can be seen that the actual spot overlap ratios of group a, b, and c experiments using the motion control optimization algorithm are all around 25%. The sample variance and the relative error relative to the ideal overlap ratio are smaller, and the relative error range is controlled within 5%. However, the average value of the actual spot overlap ratio of group d processed with a constant feed rate is 44.12%, which is a 76.48% relative error compared with the ideal overlap ratio. The sample variance of group d is also the largest.

Through the above experimental data and the physical drawing of the spherical shell machining in Fig. 11, the motion control optimization algorithm designed in this paper can effectively ensure the actual spot overlap ratio after machining. The optimized results of the actual overlap ratio relative to the theoretical value of the error can be controlled in a small range.

4 Conclusions

In this paper, a motion control optimization algorithm is proposed to optimize the surface strengthening process of nickel-based superalloy. Firstly, the processing principle of the laser shock peening of nickel alloy spherical shell parts is studied to obtain the relationship between feed rate and spot overlap ratio. The processing problem under the ideal constant feed rate is proposed to establish the influence of the curvature of the processing path curve on the amount of

Table 3 Parameters of laser shock peening processing of spherical shells

Experiment number	Radius of spherical shell (mm)	Spot diameter (mm)	Spot overlap ratio	Edge reservation (mm)	Pulse frequency (Hz)	Processing path	Motion control optimization	Pulse energy density (J)
a	50	3.5	25%	20	5	Isotropic grating	Yes	800
b	50	3.5	25%	20	5	Isotropic grating	Yes	1000
c	50	3.5	25%	20	5	Alternate grating	Yes	1000
d	50	3.5	25%	20	5	Isotropic grating	No	500

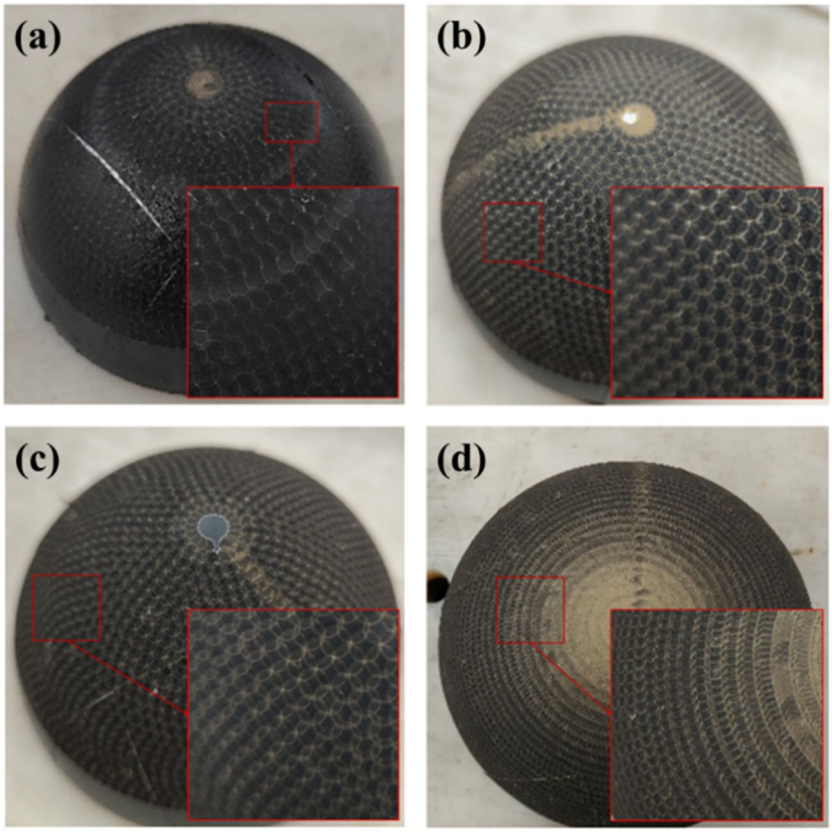

Fig. 11 Optimization algorithm processing effect

the C-axis angle. Then, the processing point trajectory program segment in the five-axis linkage machining process is decomposed, and the speed of each axis of the machine tool is checked and corrected stepwise according to the linear interpolation principle. Then the optimized equipment feed rate is obtained, and a complete motion control optimization algorithm flow is established. Finally, the feasibility of the algorithm is proved by simulation and comparison, and experimental tests are carried out on the multi-axis precision laser machining equipment to verify the excellent performance of the proposed motion control optimization algorithm. The experimental results show that the algorithm can effectively control the spot overlap ratio, and the relative error with the ideal overlap ratio is controlled within 5%.

The idea of a motion control optimization algorithm for multi-axis precision laser machining equipment studied in this paper can be extended to laser machining centers of different structural types.

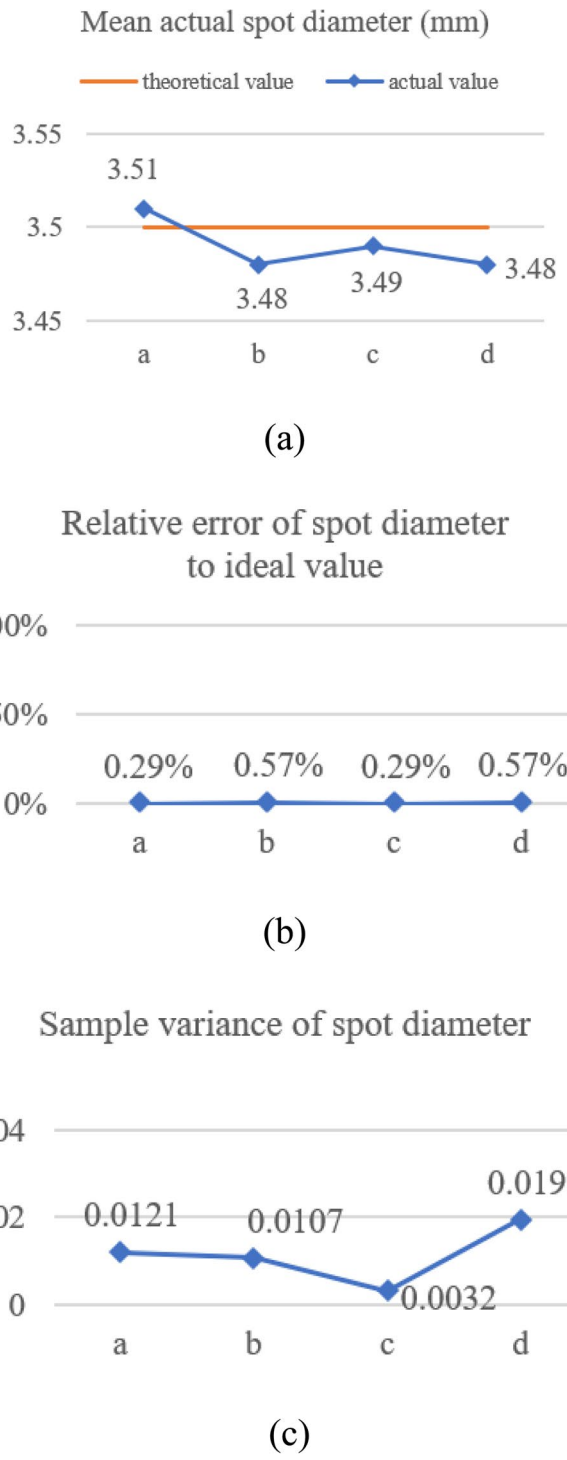

Fig. 12 Spot diameter measurement results

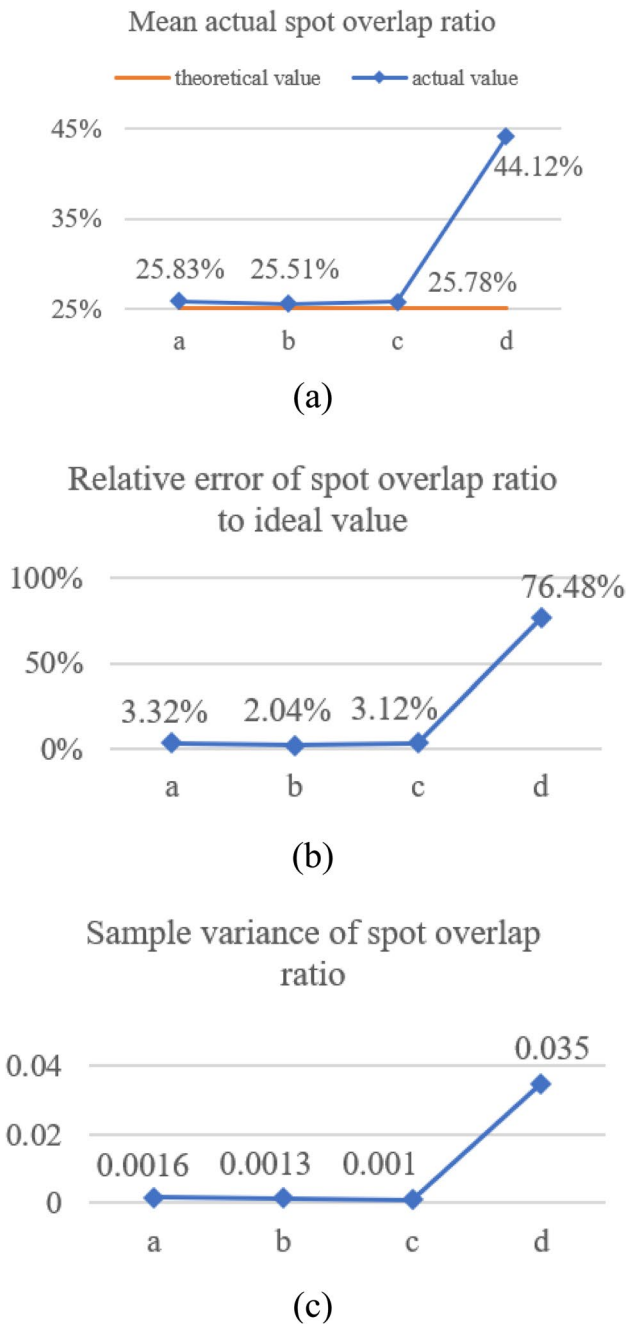

Fig. 13 Spot overlap ratio measurement results

Appendix

Spherical shell optimization feed rate comparison test processing results.

Experiment number	Mean actual spot diameter (mm)	Relative error of spot diameter to ideal value	Sample variance of spot diameter	Mean actual spot overlap ratio	Relative error of spot overlap ratio to ideal value	Sample variance of spot overlap ratio
a	3.5100	0.29%	0.0121	25.83%	3.32%	0.0016
b	3.4800	−0.57%	0.0107	25.51%	2.04%	0.0013
c	3.4900	−0.29%	0.0032	25.78%	3.12%	0.0010
d	3.4800	−0.57%	0.0196	44.12%	76.48%	0.0350

Funding This work was financially supported by the National Natural Science Foundation of China (52105424), and R&D Program of Beijing Municipal Education Commission (KM202210005033).

Declarations

Ethics approval The research does not involve ethical issues.

Consent for publication All the authors agreed to publish this paper.

Competing interests The authors declare no competing interests.

References

1. Akande IG, Oluwole OO, Fayomi OSI, Odunlami OA (2021) Overview of mechanical, microstructural, oxidation properties and high-temperature applications of superalloys. Mater Today Proc 43:2222–2231. https://doi.org/10.1016/j.matpr.2020.12.523
2. Zhang Y, Zhong Y, Cheng Y et al (2024) Microstructural evolution and micro-mechanical properties of non-isothermal solidified zone in TLP bonded Ni-based superalloy joints. J Mater Sci Technol 185:9–22. https://doi.org/10.1016/j.jmst.2023.11.006
3. Pradhan D, Shankar Mahobia G, Chattopadhyay K, Singh V (2018) Salt induced corrosion behaviour of superalloy IN718. Mater Today Proc 5:7047–7054. https://doi.org/10.1016/j.matpr.2017.11.368
4. Zhang X, Chen Y, Hu J (2018) Recent advances in the development of aerospace materials. Prog Aerosp Sci 97:22–34. https://doi.org/10.1016/j.paerosci.2018.01.001
5. Meijun L, Xu L, Zhu C, Li Z, Wei S (2024) Research progress of high entropy alloy: surface treatment improves friction and wear properties. J Mater Res Technol 28:752–773. https://doi.org/10.1016/j.jmrt.2023.12.011
6. Deng W, Wang C, Lu H, Meng X, Wang Z (2023) Progressive developments, challenges and future trends in laser shock peening of metallic materials and alloys: a comprehensive review. Int J Mach Tools Manuf 191:104061. https://doi.org/10.1016/j.ijmachtools.2023.104061
7. Ye C, Suslov S, Kim BJ, Stach EA, Cheng GJ (2011) Fatigue performance improvement in AISI 4140 steel by dynamic strain aging and dynamic precipitation during warm laser shock peening. Acta Mater 59:1014–1025. https://doi.org/10.1016/j.actamat.2010.10.032
8. Huang S, Sheng J, Wang Z et al (2020) Finite element and experimental analysis of elevated-temperature fatigue behavior of IN718 alloy subjected to laser peening. Int J Fatigue 131:105337. https://doi.org/10.1016/j.ijfatigue.2019.105337
9. Wang C, Luo K, Bu X et al (2020) Laser shock peening-induced surface gradient stress distribution and extension mechanism in corrosion fatigue life of AISI 420 stainless steel. Corros Sci 177:109027. https://doi.org/10.1016/j.corsci.2020.109027
10. Wang C, Luo K, Cai J, Lu J (2022) Obvious improvement in electrochemical and long-term immersion corrosion resistance of AISI 420 martensitic stainless steel using laser shock peening. Corros Sci 209:110688. https://doi.org/10.1016/j.corsci.2022.110688
11. Zhang C, Dong Y, Ye C (2021) Recent developments and novel applications of laser shock peening: a review. Adv Eng Mater 23:2001216. https://doi.org/10.1002/adem.202001216
12. Leap MJ, Rankin J, Harrison J, Hackel L, Nemeth J, Candela J (2011) Effects of laser peening on fatigue life in an arrestment hook shank application for Naval aircraft. Int J Fatigue 33:788–799. https://doi.org/10.1016/j.ijfatigue.2010.12.016
13. Guo W, Sun R, Song B, Zhu Y, Li F (2018) Laser shock peening of laser additive manufactured Ti6Al4V titanium alloy. Surf Coat Technol 349:503–510. https://doi.org/10.1016/j.surfcoat.2018.06.020
14. Dai FZ, Geng J, Tan WS, Ren XD, Lu JZ, Huang S (2018) Friction and wear on laser textured Ti6Al4V surface subjected to laser shock peening with contacting foil. Opt Laser Technol 103:142–150. https://doi.org/10.1016/j.optlastec.2017.12.044
15. Lu J, Lu H, Xu X, Yao J, Cai J, Luo K (2020) High-performance integrated additive manufacturing with laser shock peening – induced microstructural evolution and improvement in mechanical properties of Ti6Al4V alloy components. Int J Mach Tools Manuf 148:103475. https://doi.org/10.1016/j.ijmachtools.2019.103475
16. Geng Y, Dong X, Wang K, Yan X, Duan W (2019) Effect of microstructure evolution and phase precipitations on hot corrosion behavior of IN718 alloy subjected to multiple laser shock peening. Surf Coat Technol 370:244–254. https://doi.org/10.1016/j.surfcoat.2019.04.060
17. Fabbro R, Fournier J, Ballard P, Devaux D, Virmont J (1990) Physical study of laser-produced plasma in confined geometry. J Appl Phys 68:775–784. https://doi.org/10.1063/1.346783
18. Rubio-González C, Ocaña JL, Gomez-Rosas G, Molpeceres C, Paredes M (2004) Effect of laser shock processing on fatigue crack growth and fracture toughness of 6061–T6 aluminum alloy. Mater Sci Eng A 386:291–295. https://doi.org/10.1016/j.msea.2004.07.025
19. Lu JZ, Wu LJ, Sun GF, Luo KY, Zhang YK (2017) Microstructural response and grain refinement mechanism of commercially pure titanium subjected to multiple laser shock peening impacts. Acta Mater 127:252–266. https://doi.org/10.1016/j.actamat.2017.01.050
20. Lu JZ, Luo KY, Zhang YK, Sun GF, Gu YY (2010) Grain refinement mechanism of multiple laser shock processing impacts on ANSI 304 stainless steel. Acta Mater 58:5354–5362. https://doi.org/10.1016/j.actamat.2010.06.010
21. Fang X, Gong J, Yu Y et al (2024) Study on the fretting wear performance and mechanism of GH4169 superalloy after various laser shock peening treatments. Opt Laser Technol 170:110301. https://doi.org/10.1016/j.optlastec.2023.110301
22. Geng Y, Mo Y, Zheng H, Li G, Wang K (2021) Effect of laser shock peening on the hot corrosion behavior of Ni-based single-crystal superalloy at 750°C. Corros Sci 185:109419. https://doi.org/10.1016/j.corsci.2021.109419

23. Sheng J, Zhang H, Hu X, Huang S (2020) Influence of laser peening on the high-temperature fatigue life and fracture of Inconel 718 nickel-based alloy. Theor Appl Fract Mech 109:102757. https://doi.org/10.1016/j.tafmec.2020.102757
24. Sang Y, Yao C, Lv Y, He G (2020) An improved feedrate scheduling method for NURBS interpolation in five-axis machining. Precis Eng 64:70–90. https://doi.org/10.1016/j.precisioneng.2020.03.012
25. Sun S, Zhao P, Zhang T, Li B, Yu D (2024) Smoothing interpolation of five-axis tool path with less feedrate fluctuation and higher computation efficiency. J Manuf Process 109:669–693. https://doi.org/10.1016/j.jmapro.2023.12.012
26. Tang P-Y, Lin M-T, Tsai M-S (2022) Real-time master-based feedrate scheduling with kinematic constraints for five-axis machining. Int J Adv Manuf Technol 123:493–510. https://doi.org/10.1007/s00170-022-10172-9
27. Song D-N, Zhong Y-G, Ma J-W (2020) Look-ahead-window-based interval adaptive feedrate scheduling for long five-axis spline toolpaths under axial drive constraints. Proc Inst Mech Eng Part B J Eng Manuf 234:1656–1670. https://doi.org/10.1177/0954405420937538
28. Xu G, Luo KY, Dai FZ, Lu JZ (2019) Effects of scanning path and overlapping rate on residual stress of 316L stainless steel blade subjected to massive laser shock peening treatment with square spots. Appl Surf Sci 481:1053–1063. https://doi.org/10.1016/j.apsusc.2019.03.093
29. Lu Z, Huo G, Jiang X (2023) A novel method to minimize the five-axis CNC machining error around singular points based on closed-loop inverse kinematics. Int J Adv Manuf Technol 128:2237–2249. https://doi.org/10.1007/s00170-023-11991-0